Manganese adlayers on i-Al–Pd–Mn quasicrystal: growth and electronic structure

2009 J. Phys.: Condens. Matter 21 405005

(http://iopscience.iop.org/0953-8984/21/40/405005)

J. Phys.: Condens. Matter **21** (2009) 405005 (8pp) doi:10.1088/0953-8984/21/40/405005

Manganese adlayers on i-Al–Pd–Mn quasicrystal: growth and electronic structure

A K Shukla[1,2], R S Dhaka[1], S W D'Souza[1], M Maniraj[1], S R Barman[1], K Horn[3], Ph Ebert[4], K Urban[4], D Wu[5] and T A Lograsso[5]

[1] UGC-DAE Consortium for Scientific Research, Khandwa Road, Indore 452001, India
[2] Institut Jean Lamour, UMR 7198 CNRS—Nancy Université—UPV Metz, Département CP2S, ENS Mines Nancy, Parc de Saurupt, CS 14234, 54042 Nancy Cedex, France
[3] Fritz-Haber-Institut der Max-Planck-Gesellschaft, 14195 Berlin, Germany
[4] Institut für Festkörperforschung, Forschungszentrum Jülich GmbH, 52425 Jülich, Germany
[5] Ames Laboratory US DOE, Iowa State University, Ames, IA 50011-3020, USA

E-mail: Ajay.Shukla@mines.inpl-nancy.fr

Received 23 April 2009, in final form 17 August 2009
Published 17 September 2009
Online at stacks.iop.org/JPhysCM/21/405005

Abstract
Pseudomorphic growth of thin elemental metal films is often observed on a variety of crystalline solids. On quasicrystalline surfaces with their complex structure and the absence of translational periodicity, the situation is different since elemental metals do not exhibit quasicrystalline order, and hence the specific interaction between overlayer and substrate is decisive. Here we study the growth of manganese films on an icosahedral i-Al–Pd–Mn alloy with a view to establishing the growth mode and electronic structure. Although we observe an exponential intensity variation of the adlayer and substrate related x-ray photoemission spectroscopy (XPS) peaks, low energy electron diffraction (LEED) shows that Mn adlayers do not exhibit quasicrystallinity. The detailed structure of the Mn 2p core level line reveals considerable electronic structure differences between the quasicrystalline and elemental metal environment. Evidence of a substantial local magnetic moment on the Mn atoms in the overlayer (about 2.8 μ_B) is obtained from the Mn 3s exchange splitting.

1. Introduction

The aperiodic ordering in the quasicrystalline alloys (QCs) and their unusual properties have fascinated condensed matter physicists ever since their discovery, as the presence of the aperiodicity and perfect atomic order seem to defy well-established concepts of solid state physics [1]. QCs are mostly three-component alloys and the chemical and structural complexities are a challenge for an understanding of their physical properties. Within the last few years, considerable efforts have focused on finding QCs with a less complex chemical composition. So far, no quasicrystalline order has been found in the elements. By imposing such order in the elemental metal films grown on clean and well-ordered QC surfaces, quasiperiodic ordering in such films has indeed been observed [2–4]. Such films are of particular interest as they provide an opportunity to study the influence of quasiperiodic ordering on the electronic structure in the elements.

The results to date from the growth of different metal adlayers on QCs can be divided into three categories: (a) heterogeneous nucleation of adatoms resulting in island growth; (b) pseudomorphic growth resulting in single element quasicrystalline film; and (c) cubic domains of deposited material having an orientational relationship with the quasicrystal substrate [5, 6]. Earlier, we have studied the growth and electronic structure of alkali metal (Na and K) adlayers on icosahedral i-Al–Pd–Mn using x-ray photoemission spectroscopy (XPS) [7]. This work showed that below one monolayer (1 ML), both Na and K form a dispersed phase on i-Al–Pd–Mn and there is hardly any charge transfer to the substrate. The variation of the adlayer and substrate core level intensities with coverage indicated layer-by-layer growth.

This study motivated Krajčí and Hafner to perform *ab initio* density functional method based theoretical calculations for the alkali metal (Na and K) on the i-Al–Pd–Mn surface [8]. They found that a monolayer of Na and K grows pseudomorphically on a QC and predicted that the quasiperiodic order may propagate to the alkali metal bilayer. Recently, using low electron diffraction (LEED), we have shown that Na and K form a highly regular quasiperiodic monolayer on i-Al–Pd–Mn and that the quasiperiodicity propagates up to the second layer in Na in agreement with theory [9].

These results raise the obvious question of whether a similar growth mode can be found in transition metals, such as the constituents Pd and Mn in the case of the most intensely studied icosahedral i-QCs, i.e. Al–Pd–Mn. In contrast to free electron like alkali metals, the electronic structure of 3d transition metals is more complicated due to their magnetic properties and correlation effects. Growth of ultrathin transition metal adlayers is a subject of current research because of their possible applications in magnetic recording, spintronic devices, etc [10]. In recent years, different transition metals (Co, Ni, Fe) have been deposited on i-Al–Pd–Mn in search of magnetic ordering on an essentially diamagnetic QC surface [11–13]. However, until now, pseudomorphic growth of any magnetic transition metal has not been observed.

Weisskopf *et al* have studied the growth of Fe on i-Al–Pd–Mn deposited at 340 K [11]. They found that, up to 4 ML of Fe, the surface layers do not show structural or magnetic ordering. In this regime, it was deduced that Fe atoms diffuse and intermix with the substrate. From 4 to 8 ML, Al inter-diffusion with the Fe overlayer was found to cause a structural transformation to five domains of a cubic structure. For Fe overlayers greater than 8 ML, pure Fe was found to grow in five domains having an orientational relationship with the substrate, with some tilting of the domains away from the surface normal. For Ni on i-Al–Pd–Mn at room temperature, intermixing of Ni and Al was observed and for higher Ni coverages, formation of five cubic domains rotated azimuthally by 72° with respect to each other and aligned with symmetry directions of i-Al–Pd–Mn were observed [12]. For Co growth on i-Al–Pd–Mn, intermixing was not observed and the formation of five cubic domains of Co having an orientational relationship with the i-Al–Pd–Mn substrate were observed even in the sub-monolayer Co coverage [13]. Mn is an interesting candidate for transition metal growth due to its large local magnetic moment. Mn might also be an interesting candidate for pseudomorphic growth on i-Al–Pd–Mn, since it is one of the elemental constituents of the quasicrystal substrate.

The asymmetric line shape of the Mn 2p core level has been well studied for i-Al–Pd–Mn, Al–Mn alloys and Mn metal [14, 15, 17, 18]. The Mn 2p core level of i-Al–Pd–Mn has been found to be much less asymmetric than that for Mn metal and it has been related to the pseudogap (decrease in the density of states around the Fermi level) in the i-Al–Pd–Mn [15]. Recently, we have studied the Mn 2p core level of bulk-like Mn film using high-resolution photoemission spectroscopy and an unusual satellite feature at 1 eV higher binding energy (BE) than the main peak has been observed [17]. It originates due to the intra-atomic multiplet effect related to Mn atoms with large local moment [17]. This satellite feature was not observed in the Mn 2p core level of i-Al–Pd–Mn and Al–Mn alloys [14, 15, 18]. It would be interesting to investigate whether a 1 eV satellite can be observed in Mn films grown on i-Al–Pd–Mn. Exchange splitting of the Mn 3s core level provides an estimation of the average local magnetic moment of Mn atoms in Mn adlayers [19–22].

Here, we report the growth and electronic structure of Mn adlayers on the five-fold surface of i-Al–Pd–Mn using XPS and LEED. The LEED patterns recorded as a function of Mn coverage demonstrate that Mn adlayers are not quasicrystalline and do not have long-range order. An increase in binding energy and full width at half-maximum (FWHM) of the Mn 2p core level with increasing Mn coverage is observed. An extra feature at about 1 eV higher BE with respect to the Mn $2p_{3/2}$ peak emerges with adlayer coverage. The change in the relative intensity of the 1 eV feature as a function of Mn coverage has been determined, which explains the observed changes in the FWHM of Mn 2p core level with coverage. The exchange splitting of the Mn 3s core level increases at lower coverage compared to thick Mn film, which indicates that the local magnetic moment of Mn is higher at lower coverage.

2. Experimental details

A single grain i-Al–Pd–Mn quasicrystal with bulk composition $Al_{69.4}Pd_{20.8}Mn_{9.8}$ was grown using the Bridgman technique [23, 24]. The base pressure of the experimental ultra-high vacuum chamber was 6×10^{-11} mbar. A commercial electron energy analyzer (Phoibos 100 from Specs GmbH, Berlin, Germany) and a Mg Kα x-ray source have been used for the XPS measurements with an overall energy resolution of about 0.8 eV. LEED experiments have been performed using four-grid rear view ErLEED optics. The polished i-Al–Pd–Mn surface was cleaned by repeated cycles of Ar^+ sputtering and annealing up to 870–900 K. Surface composition and cleanliness were checked by recording the Al 2p, Pd 3d, Mn 2p, and O KLL Auger signals. Mn adlayers were deposited on i-Al–Pd–Mn at a sample temperature of 130–150 K by using a water cooled Knudsen-type effusion cell operated at 823 K [25]. During the deposition, the chamber pressure rose to 1.5×10^{-10} mbar. The substrate is held at low temperatures (130–150 K) for deposition and measurements. Such temperatures are used to avoid possible intermixing of the adlayer with the substrate, which has been observed at room temperature in Mn adlayers on Al [26, 27]. The thickness of the adlayers was calculated from the area under the adlayer (Mn 2p) and the substrate related (Al 2p) core levels after x-ray satellite and Tougaard background subtraction [7, 25]. These spectra are recorded under similar conditions, for example, analyzer settings, x-ray source intensity, sample position, etc. After deposition of the Mn adlayer, the Mn 2p signal comes from Mn film as well as substrate as i-Al–Pd–Mn contains Mn. However, to calculate the coverages, we have subtracted the Mn 2p signal of a clean substrate from the total (film + substrate) Mn 2p signal. The Doniach–Šunjić (DS) [29] line shape function

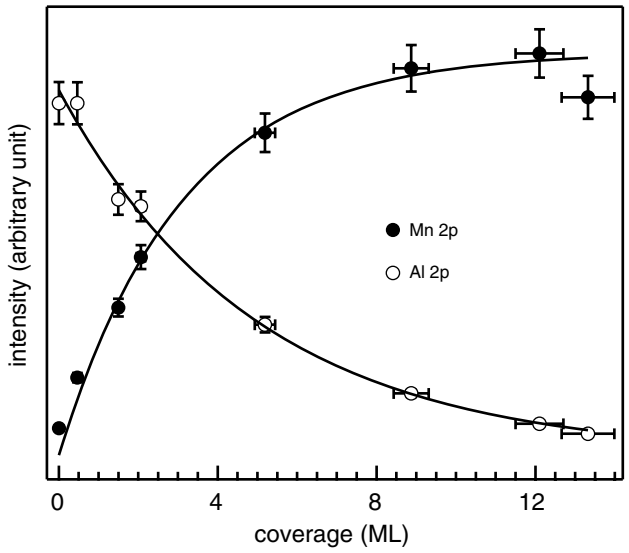

Figure 1. Variation of Mn 2p (filled circle) and Al 2p (unfilled circle) core level intensities as a function of coverage, solid lines are fit to data. The uncertainty (±5%) in the coverage and intensity is indicated by the error bars.

has been used in the literature to simulate Mn 2p core level considering the core level peak as a single component [14, 15].

One monolayer ($c = 1$ or 1 ML) is defined to be a close packed Mn layer that completely covers the i-Al–Pd–Mn surface [7, 16]. We have calculated the deposition rate from the relative intensities of the substrate Al 2p and the adlayer Mn 2p areas. The details of the method are given in [25]. The intensity of the substrate signal depends on the inelastic mean free path of the photoelectrons and the thickness of the adlayer [28]. The Mn deposition rate was 0.13 ± 0.02 ML min^{-1}.

3. Results and discussion

In order to ascertain the growth mode, we analyze in figure 1 the variation in adlayer (Mn 2p) and substrate (Al 2p) core level integrated intensity for Mn/i-Al–Pd–Mn, as a function of coverage. The substrate signal decreases with increase in the thickness of adsorbed layers as emitting photoelectrons suffer extra inelastic scattering. The intensity of the substrate signal (I_S) after n ML deposition is given by [28],

$$I_S = I^S_\infty[\exp(-nd/\lambda^m_A(E_S)\cos\theta)] \quad (1)$$

where I^S_∞ is the substrate signal without deposition, d is the thickness of one monolayer and $\lambda^m_A(E_S)$ is the inelastic mean free path of photoelectrons emitted from the substrate (Al 2p) in the adsorbate. E_S is the kinetic energy of Al 2p photoelectrons. The adlayer signal (I_A) is given by,

$$I_A = I^A_\infty[1 - \exp(-nd/\lambda^m_A(E_A)\cos\theta)] \quad (2)$$

where I^A_∞ is the intensity for the bulk adlayer material. I_S and I_A are extracted by calculating the area under the Al 2p and Mn 2p peaks. I^S_∞ and I^A_∞ are taken to be the photoionization cross-sections of Al 2p and Mn 2p, respectively [30]. E_A is the kinetic energy of Mn 2p photoelectrons, and $\lambda^m_A(E_A)$ is the inelastic mean free path of Mn 2p photoelectrons in the adsorbate. θ is the emission angle of the photoelectrons with respect to the surface normal, which is 50° in our case. We have fitted the Al 2p and Mn 2p intensity variation using equations (1) and (2), and $\lambda^m_A(E_S)$ and $\lambda^m_A(E_A)$ are treated as adjustable parameters. The best fit is obtained for $\lambda^m_A(E_S) = 7.6$ ML and $\lambda^m_A(E_A) = 4.8$ ML. The exponential intensity variation of Mn 2p and Al 2p excludes the possibility of island and layer-island growth. From the present data, the growth mode can be termed as pseudo-layer-by-layer [31], where the second layer starts growing before completion of the first layer. Pseudo-layer-by-layer growth has been reported on the basis of exponential variation of adsorbate and substrate intensity [31].

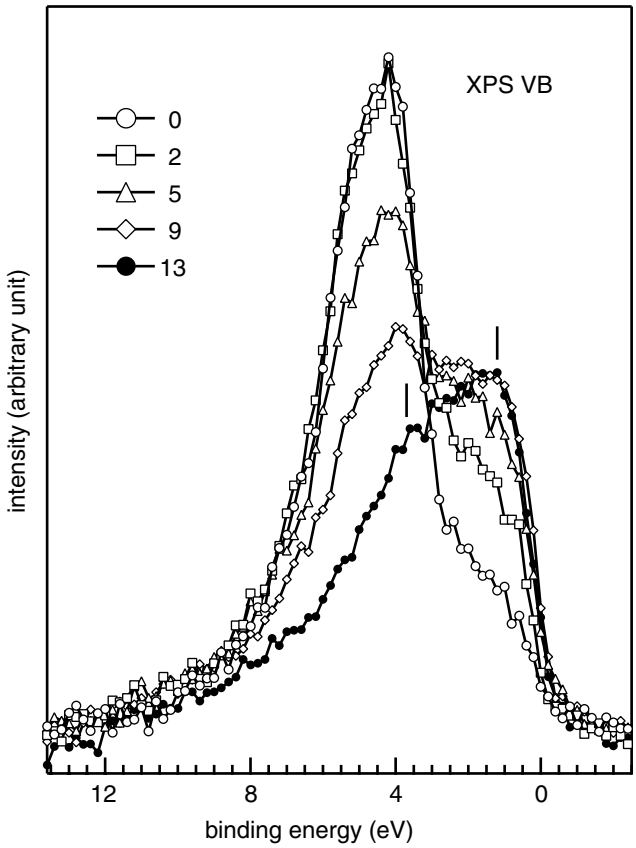

Figure 2. XPS valence band spectra of Mn/i-Al–Pd–Mn as a function of Mn adlayer thickness.

The XPS valence band spectra for Mn/i-Al–Pd–Mn are shown in figure 2. For i-Al–Pd–Mn, the main peak centered around 4 eV is related to the Pd 4d states and the spectral intensity near E_F is mainly due to Mn 3d-Al s, p hybridized states [15]. The intensity of the Pd 4d related peak diminishes gradually with a slight shift toward lower BE that is indicative of the appearance of Mn 3d related states of the bulk Mn valence band. For 13 ML Mn, the valence band exhibits a peak at 1.1 eV with a shoulder at 3.8 eV (ticks in figure 2) that resembles bulk Mn [32]. In fact, the gradual transformation of the i-Al–Pd–Mn valence band to the Mn valence band with the absence of any other feature is consistent with the exponential variation of the intensities of the substrate Al and adlayer Mn 2p core level spectra (figure 1).

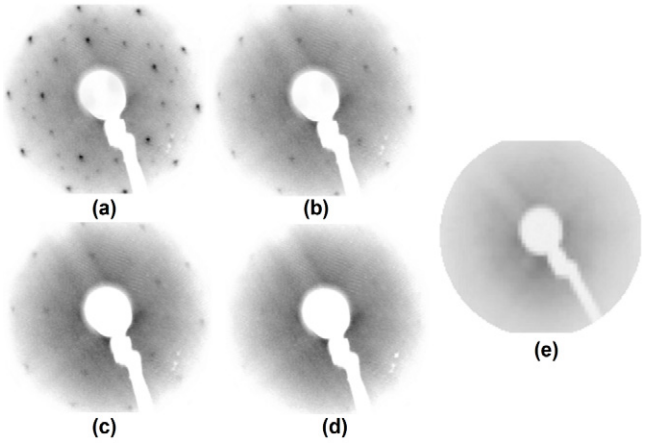

Figure 3. LEED patterns recorded at 78 eV electron energy at near normal incidence for (a) clean, (b) 0.4 ML, (c) 0.6 ML, (d) 0.8 ML, and (e) 13 ML Mn adlayer. Images are shown in inverted gray scale where black indicates highest brightness.

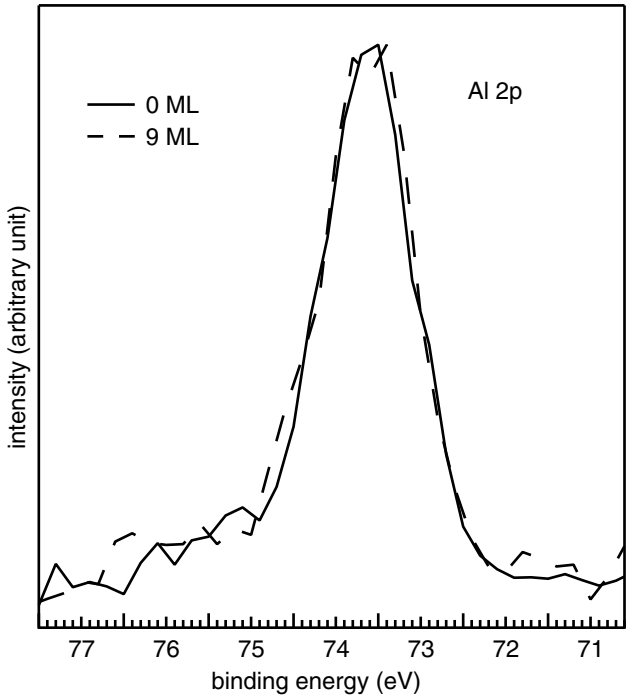

Figure 4. Comparison between Al 2p photoelectron spectra for clean Al (solid line) and after deposition of 9 ML Mn layer (dashed line) on i-Al–Pd–Mn at 130 K. Spectra have been normalized to have the same peak height.

Structural information on layer growth can be derived from the LEED pattern of Mn/i-Al–Pd–Mn for different coverages shown in figure 3. For the clean surface (figure 3(a)), the LEED pattern shows the characteristic five-fold symmetry with sharp diffraction spots, which confirms the quasicrystallinity of the studied surface. We observe an inner and outer ring consisting of ten sharp spots. Closer inspection of the spot intensities reveals two inequivalent sets of five spots, which exhibit five-fold symmetry. In principle, the reciprocal space of quasicrystals is densely filled due to their aperiodic order. However, diffraction spots which follow τ-scaling have the prominent intensity compared to others [33]. Between the inner and outer ring, some other spots with weaker intensity are also observed, which we refer to as intermediate spots. With increasing Mn coverage, we observe a continuous fading out of the LEED pattern; there is a uniform background for the $\geqslant$0.8 ML Mn adlayer and the spots are no longer visible. For as low as 0.4 ML, many of the spots cease to exist (figure 3(b)). For thicker Mn adlayers (1–13 ML), the LEED shows a uniform background with no spots. Figure 3 clearly shows that intermediate spots fade earlier than inner and outer ring spots with increasing Mn coverage due to their weaker intensity. Although XPS indicates that Mn growth is pseudo-layer-by-layer, the disappearance of the LEED spots indicates the layers do not exhibit the long-range order of the quasicrystalline surface and are disordered. Multi-site adsorption of Mn atoms may be the reason for the destruction of quasiperiodicity of the i-Al–Pd–Mn substrate for sub-monolayer coverages of the Mn adlayer. A similar progressive extinction of LEED has been observed for low coverages of Fe, Ni, and Co deposited on i-Al–Pd–Mn where the adlayers are not quasicrystalline [11–13].

We have not observed any significant change in the peak positions and line shape of substrate related (Al 2p and Pd 3d) core levels as a function of Mn coverage. Continuous decrease of substrate core level intensities is observed with increasing Mn coverage and substrate signal was not visible for 13 ML Mn coverage. In our earlier study, we have investigated the growth of Mn on Al(111) at *room temperature* [26]. It has been found that the FWHM of the Al 2p peak increases with the increase in Mn layer thickness and becomes more asymmetric on the lower BE side. The difference spectrum between clean Al 2p and for 3.5 ML Mn shows a peak at the lower BE (72.5 eV) with respect to the Al 2p peak for 3.5 ML. It was related to the asymmetry of the Al 2p peak towards lower BE with Mn deposition. Broadening in Al 2p towards the lower BE side has been related to the intermixing of Mn adatoms with Al(111) substrate [26]. The difference spectra between different Mn coverages and clean Al show that this extra component shifts to lower BE and also increases in intensity with increasing Mn coverage. Figure 4 shows the Al 2p spectra for clean i-Al–Pd–Mn and for 9 ML Mn deposition on i-Al–Pd–Mn at 130 K. It clearly shows that there is no extra broadening in the Al 2p core level after Mn deposition on i-Al–Pd–Mn at 130 K. It indicates that there is no intermixing of Mn adatoms with the i-Al–Pd–Mn substrate.

The Mn 2p spectra in figure 5 show the spin–orbit split $2p_{3/2}$ and $2p_{1/2}$ core level peaks with a splitting of about 11 eV. For the clean i-Al–Pd–Mn surface, the Mn $2p_{3/2}$ peak appears at 638.6 eV BE. The intensity of the Mn 2p core level increases and also shifts toward higher BE with increasing coverage. The total shift in the BE of Mn $2p_{3/2}$ up to 5 ML is 0.2 ± 0.05 eV, as shown on an expanded energy scale in the inset of figure 5. Above 5 ML, there is hardly any shift in BE. A similar variation of the 2p core level BE has been observed for Mn/Al and Co/Al [26, 34]. For the highest coverage of 13 ML, the Mn $2p_{3/2}$ peak appears at 638.8 eV, which is in good agreement with the BE position of Mn $2p_{3/2}$ (638.8 eV) for a 75 ML thick Mn layer on Al(111) [26]. A lower BE in i-Al–Pd–Mn

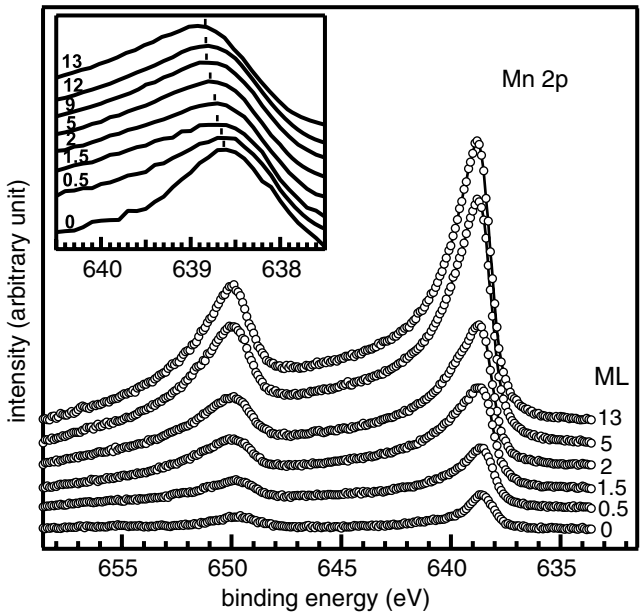

Figure 5. Mn 2p core level spectra as a function of coverage. The spectra have been shifted along the vertical axis for clarity of presentation. The inset shows the shift in binding energy of the Mn $2p_{3/2}$ core level peak on an expanded scale. Spectra shown in the inset are normalized to the same height and the peak positions are indicated by tick marks.

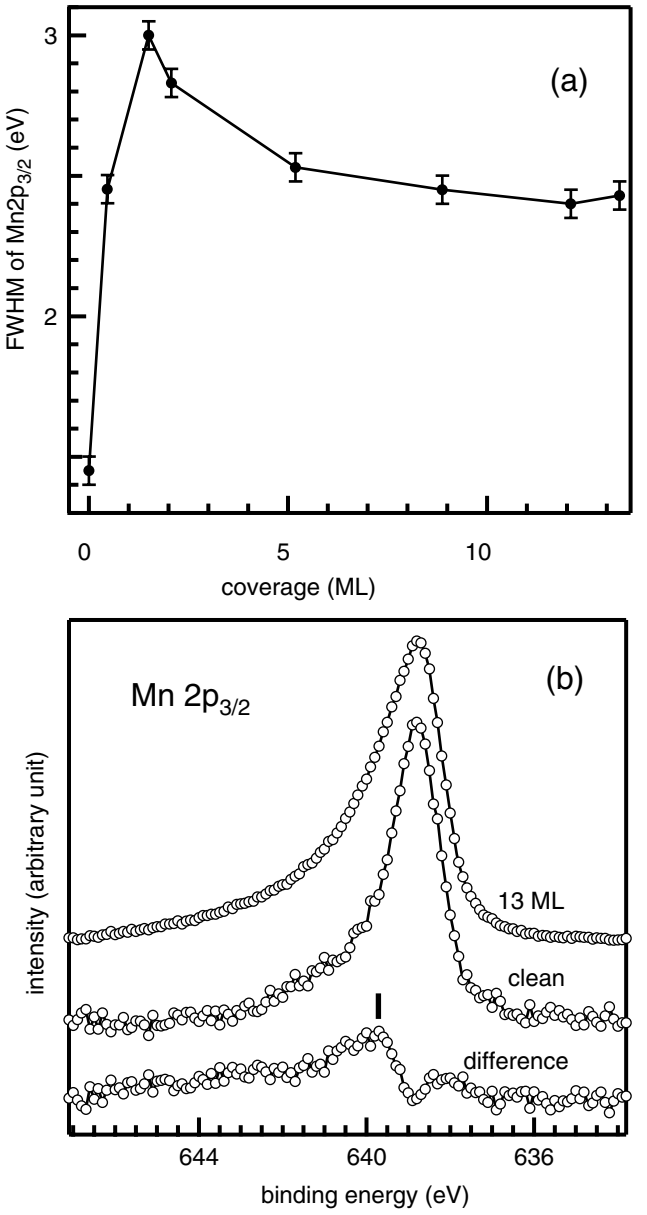

Figure 6. (a) Variation of the FWHM of the Mn $2p_{3/2}$ peak as a function of Mn coverage. (b) Mn $2p_{3/2}$ core level peak for 13 ML Mn layer and clean i-Al–Pd–Mn. The intensity is normalized with respect to the Mn $2p_{3/2}$ peak. The difference spectrum between the Mn $2p_{3/2}$ peak for 13 ML Mn layer and clean i-Al–Pd–Mn (shifted to same peak position) is shown. The spectra have been shifted along the vertical axis for clarity of presentation.

possibly occurs because of the efficient screening of the Mn 2p core–hole in the photoemission final state by the Al s, p conduction electrons. Another possible reason could be the redistribution of charges in the initial state through Mn 3d-Al 3s, p hybridization. As the Mn coverage increases, these substrate related effects become weaker and the BE increases to reach the metallic Mn value. Unfortunately, no calculations are available to distinguish between the two factors.

We do not observe any correlation-induced charge transfer satellite in the Mn 2p spectrum. The correlation-induced charge transfer satellite has been observed earlier in the Mn 2p spectra for 0–2 ML Mn adlayers grown on different transition and noble metals at 4–5 eV higher binding energy than the main peak [35–37]. So, one might expect this satellite also here since about 20% of Al–Pd–Mn consists of Pd and Mn. The reason for the absence of this type of satellite in the Mn 2p spectra of Mn/i-Al–Pd–Mn can be understood on the basis of our earlier work on Mn/Al [17]. These satellites have been shown to exist only when the hybridization is weak [17]. In the present case, substantial Al 3s, p-Mn 3d hybridization in i-Al–Pd–Mn suppresses these satellites. For the Mn adlayers, since the top layer of i-Al–Pd–Mn is Al-rich [38, 39], the situation is quite similar to Mn/Al where s, p-d hybridization suppresses the charge transfer satellites [17].

Here, we concentrate on the shape of the Mn 2p core level peak and the information on the electronic structure of the adlayer that can be obtained from it. Figure 6(a) shows the variation in the FWHM of the Mn $2p_{3/2}$ peak as a function of Mn coverage. The FWHM of the Mn $2p_{3/2}$ peak of clean i-Al–Pd–Mn is 1.45 eV, which increases to 2.45 eV for 0.5 ML Mn coverage. The maximum FWHM (3 eV) is observed for a 1.5 ML Mn layer; for higher coverages it starts decreasing and reduces to 2.45 eV for 5 ML and remains similar for thicker layers. In figure 6(b), we show that there is a clear difference in the Mn $2p_{3/2}$ line shape for the highest Mn coverage (13 ML) and clean i-Al–Pd–Mn; this is highlighted by the difference spectrum (figure 6(b)). The Mn $2p_{3/2}$ peak for 13 ML Mn is notably asymmetric toward higher BE compared to i-Al–Pd–Mn. Thus, the difference spectrum shows a peak at 639.5 eV, about a 1 eV higher BE than the main peak position. The difference spectrum of two spectra may give rise to fictitious features if the energy position of the peak in the spectra is not the same. Therefore, we have shifted the clean Mn 2p spectra to have the same energy position of Mn

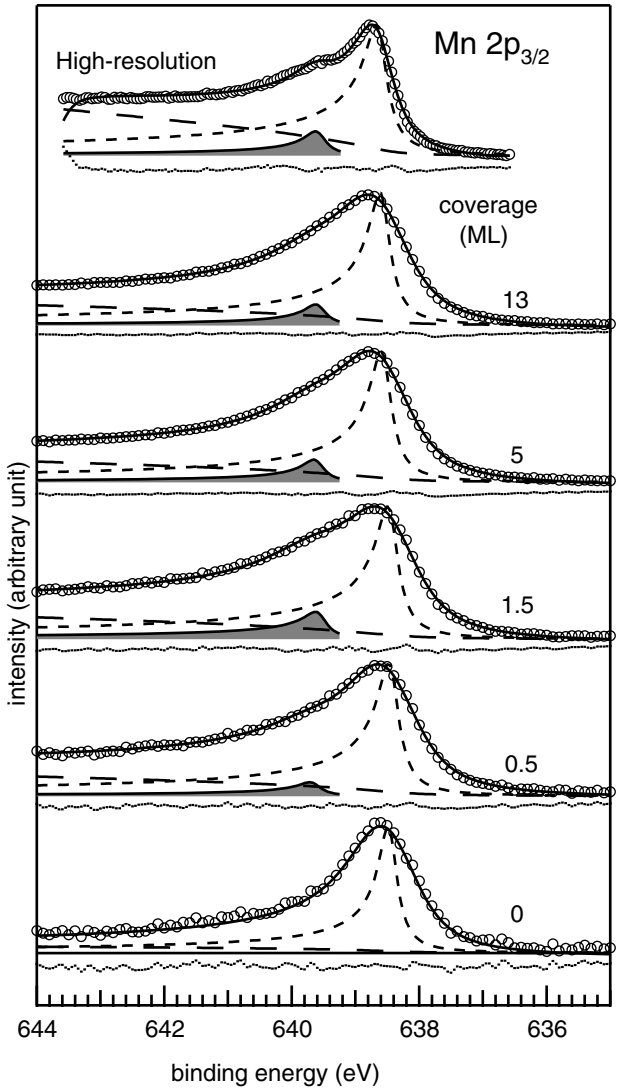

Figure 7. Mn $2p_{3/2}$ peak as a function of coverage. Experimental data are shown as unfilled circles. The simulated spectra (thick solid line), deconvoluted main peak (short dashed line), 1 eV feature (shaded), the inelastic background (long dashed line), and the residue (dots) obtained from least-square fitting are shown. The top spectrum is a high-resolution Mn $2p_{3/2}$ spectrum for a thick Mn adlayer on Al from [16]. The spectra have been shifted along the vertical axis for clarity of presentation.

2p as a 13 ML Mn film and then the difference spectrum has been obtained. Interestingly, the position of the peak in the difference spectrum coincides with a satellite in the Mn 2p spectrum of Mn, as shown by high-resolution Mn $2p_{3/2}$ spectra for a thick Mn adlayer on Al (top spectrum, figure 7) [17]. Thus, the difference spectrum in figure 6(b) demonstrates the presence of the satellite in the Mn/i-Al–Pd–Mn adlayer from raw data without any curve fitting.

The presence of the peak in the difference spectrum that coincides with the satellite peak of Mn and the observed changes in the FWHM of Mn $2p_{3/2}$ peak (figure 6(a)) prompted us to perform a least-square fitting of the Mn $2p_{3/2}$ core level at different Mn coverages, as shown in figure 7. The high-resolution (0.37 eV) Mn $2p_{3/2}$ spectrum obtained using synchrotron radiation (top spectrum in figure 7), was fitted using two DS functions corresponding to the main peak and the 1 eV satellite [17, 15, 14]. For fitting the Mn/i-Al–Pd–Mn data recorded with our laboratory x-ray source, the same DS line shape (peak position, DS asymmetry parameter α, lifetime broadening 2γ) was used. Thus, we obtain a reliable fit for the XPS data based on the higher-resolution synchrotron data [17, 18]. We found that the spectra for the 13 ML Mn/i-Al–Pd–Mn cannot be simulated by a single Doniach–Šunjić line shape, and a second component is required [17, 18]. The position of the second component is varied, and the best fit is obtained for a separation of about 1 eV from the main peak. The simulated spectra and the residual show the good quality of the fit. The second component (see figure 7, shaded) corresponds to the Mn 2p satellite. For a 13 ML Mn film, which is representative of bulk-like Mn, we find $\alpha = 0.32$ and $\gamma = 0.17$ for the main peak, and the satellite is clearly observed. The satellite originates from an intra-atomic multiplet effect, particularly the 2p–3d exchange, and its intensity is correlated with the local magnetic moment of Mn [17]. α and γ are in good agreement with the values obtained from high-resolution Mn 2p core level data (top spectrum, figure 7) [17]. Fournée *et al* reported a considerably higher α (=0.46) for bulk Mn metal from XPS data [15]. The overestimation in α for Mn metal [15] is probably due to the fact that the 1 eV satellite was not considered while simulating the Mn 2p line shape [17]. The intensity of the satellite is negligible for the i-Al–Pd–Mn substrate and α for the main peak turns out to be 0.24. This line shape is in agreement with high-resolution data reported in the literature [14]. For i-Al–Pd–Mn, a significant Al 3s, p-Mn 3d hybridization would result in a suppression of the 1 eV satellite [17]. Note that α for i-Al–Pd–Mn (0.24) is smaller than that of Mn metal (0.32). This has been related to the low density of states at the Fermi level in the former due to the presence of the pseudogap [15].

The satellite to main peak area ratio, as determined from least-square fitting is shown as a function of Mn coverage in figure 8. The satellite intensity jumps to the highest value (0.25) around 1 ML, and then decreases gradually as coverage increases and saturates around 0.16. The uncertainty in the determination of the satellite intensity for lowest coverage (0.5 ML) may be larger than those at higher coverages. If we compare figures 8 and 6(a), a striking similarity of the variation in FWHM and the relative intensity of the satellite is observed. This shows that the variation of FWHM occurs due to the change of the unresolved satellite intensity.

The satellite intensity variation shown in figure 8 can be related to the change in the Al 3s, p-Mn 3d and Mn 3d-Mn 3d hybridizations with Mn coverage. At the i-Al–Pd–Mn surface, Al 3s, p states are strongly hybridized with Mn 3d states. Thus, for deposition of sub-monolayer Mn on i-Al–Pd–Mn, Mn adatom 3d states are strongly hybridized with the substrate related Al 3s, p states since i-Al–Pd–Mn has an Al-rich top layer. This results in a weaker intensity of the satellite for low coverages like 0.5 ML. However, above 1 ML Mn coverage, Mn adatoms in the second layer are no longer in direct contact with the Al-rich substrate; thus the overall influence of Al 3s, p-Mn 3d hybridization starts to decrease with the buildup of the

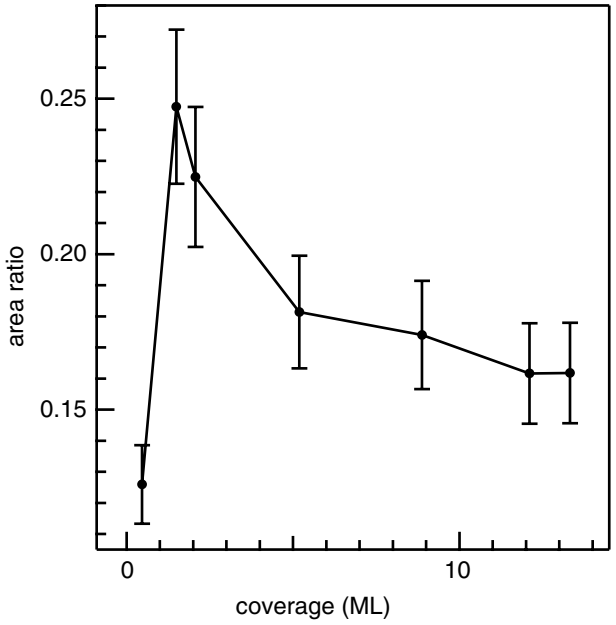

Figure 8. The satellite to the main peak intensity ratio obtained from the least-square fitting (figure 6) of Mn $2p_{3/2}$, as a function of Mn coverage. Error bars are also shown.

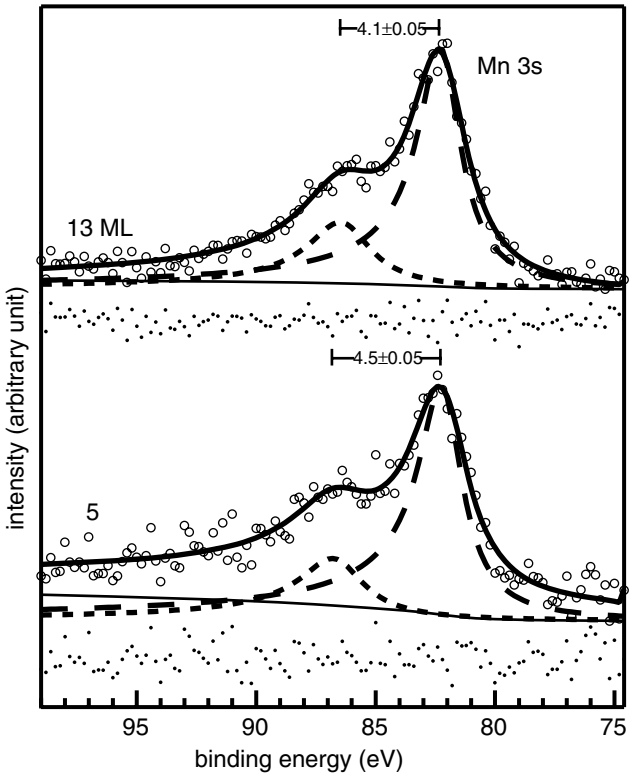

Figure 9. Mn 3s core level spectra (unfilled circles) for 13 and 5 ML are shown. The simulated spectra (thick solid line), deconvoluted ^{7}S (long dashed line), ^{5}S (short dashed line) peak, the iterative background (thin solid line), and the residual (dots) obtained from least-square fitting are shown. The separation between ^{7}S and ^{5}S peaks is indicated.

second layer. Consequently, the satellite intensity increases for 1.5 ML. As the layer thickness further increases, the influence of Mn 3d–Mn 3d hybridization naturally increases and this leads to the gradual decrease of the satellite intensity that tends toward the bulk value of 0.17 [17].

The decrease in the satellite intensity in Mn/Al has been shown to result in a concomitant decrease in the Mn magnetic moments, although a quantitative estimate of the moments was not possible [17]. So, to obtain a quantitative estimate of the Mn magnetic moments, we have studied the Mn 3s core level spectra. However, here the analysis of the Mn 3s line is complicated by the Al plasmon loss structures [26, 40]. The surface and bulk plasmon energies corresponding to the Al 2p core level coincide with the Mn 3s line, which makes it difficult to clearly observe the latter at low Mn coverages (<5 ML). Hence, we have subtracted the plasmon region of Al 2p for i-Al–Pd–Mn from the Mn 3s spectrum recorded after Mn deposition to observe the Mn 3s peak only. In figure 9, Mn 3s core level spectra, extracted in this way, for 5 and 13 ML Mn/i-Al–Pd–Mn are shown. The Mn 3s peak is split into two components, due to the exchange interaction between the 3s photohole and the unpaired 3d electrons [41]. Two final states (^{7}S and ^{5}S) may be reached by photoemission from the 3s shell.

The Mn 3s spectra have been fitted and the simulated spectra with both the components, iterative background, and the residual as obtained from the fitting are shown in figure 9. The exchange splitting (energy separation between ^{7}S and ^{5}S) of 4.1 ± 0.05 eV observed for a 13 ML Mn layer is in good agreement with the exchange splitting (4.08 eV) observed for thick α-Mn films [19]. The exchange splitting turns out to be 4.5 ± 0.05 eV for 5 ML. From the spin resolved Fe 3s spectrum, which also exhibits a doublet structure, Hillebrecht *et al* showed that the electrons in the high BE peak (^{5}S) have majority spin character, while electrons at the low BE peak (^{7}S) have minority spin character [42]. The exchange splitting of Mn 3s is therefore a measure of the d-band moment and should increase with the local magnetic moment [43]. Since the local magnetic moment should be larger for higher exchange splitting, we infer from the Mn 3s spectra that the average magnetic moment of Mn is larger for 5 ML compared to 13 ML. McFeely *et al* derived the Mn local moment to be 2.5 μ_B corresponding to 4.08 eV exchange splitting [19]. Following their approach, we find the Mn local moment to be about 2.8 ± 0.03 μ_B, corresponding to a 4.5 eV exchange splitting. The decrease in Mn magnetic moment at higher coverage is consistent with the decrease in the satellite intensity with increasing coverage (figure 8), as shown in reference [17]. An increase in the local magnetic moment of Mn atoms at lower coverages has also been observed for other systems, such as Mn/Ir(111) [20].

4. Conclusions

Although the Mn adlayer (Mn 2p) and substrate i-Al–Pd–Mn (Al 2p) XPS peaks exhibit exponential intensity variation, LEED shows that the Mn adlayers on i-Al–Pd–Mn do not exhibit quasicrystalline growth. The valence band spectra show the emergence of Mn 3d related states and gradual suppression of the Pd 4d peak with increasing Mn coverage. The Mn $2p_{3/2}$

core level asymmetry changes with coverage, as shown by the variation of the FWHM. We show that the FWHM variation is actually related to a satellite at about 1 eV higher BE from the main peak. We relate the characteristic intensity variation of the satellite to the change in Al 3s, p-Mn 3d and Mn 3d–Mn 3d hybridization. From the exchange splitting of Mn 3s, we find that the local magnetic moment of Mn is higher at lower coverage.

Acknowledgments

The work has been performed through funding from D S T - Max Planck Institute Partner Group project and Ramanna Research Grant. AKS acknowledges support from the Chemistry Department of Centre National De La Recherche Scientifique, France. DW and TAL acknowledge support from the US Department of Energy, Basic Energy Sciences under Contract No. De-AC02-07CH11358.

References

[1] Shechtman D, Blech I, Gratias D and Cahn J W 1984 *Phys. Rev. Lett.* **53** 1951
[2] Franke K J, Sharma H R, Theis W, Gille P, Ebert Ph and Rieder K H 2002 *Phys. Rev. Lett.* **89** 156104
[3] Ledieu J, Hoeft J T, Reid D E, Smerdon J A, Diehl R D, Lograsso T A, Ross A R and McGrath R 2004 *Phys. Rev. Lett.* **92** 135507
[4] Sharma H R, Shimoda M, Ross A R, Lograsso T A and Tsai A P 2005 *Phys. Rev.* B **72** 45428
[5] Fournée V and Thiel P A 2005 *J. Phys. D: Appl. Phys.* **38** R83
[6] Sharma H R, Shimoda M and Tsai A P 2007 *Adv. Phys.* **56** 403
[7] Shukla A K, Dhaka R S, Biswas C, Banik S, Barman S R, Horn K, Ebert Ph and Urban K 2006 *Phys. Rev.* B **73** 054432
[8] Krajčí M and Hafner J 2007 *Phys. Rev.* B **75** 224205
[9] Shukla A K, Dhaka R S, D'Souza S W, Singh S, Wu D, Lograsso T A, Krajčí M, Hafner J, Horn K and Barman S R 2009 *Phys. Rev.* B **79** 134206
[10] Demangeat C and Parbelas J C 2002 *Rep. Prog. Phys.* **65** 1679
[11] Weisskopf Y, Luscher R and Erbudak M 2005 *Surf. Sci.* **578** 35
[12] Weisskopf Y, Erbudak M, Longchamp J N and Michlmayr T 2006 *Surf. Sci.* **600** 2592
[13] Weisskopf Y, Burkardt S, Erbudak M and Longchamp J N 2007 *Surf. Sci.* **601** 544
[14] Horn K, Theis W, Paggel J J, Barman S R, Rotenberg E, Ebert Ph and Urban K 2006 *J. Phys.: Condens. Matter* **18** 435
[15] Fournée V, Pinhero P J, Anderegg J W, Lograsso T A, Ross A R, Canfield P C, Fisher I R and Thiel P A 2000 *Phys. Rev.* B **62** 14049
Fournée V, Anderegg J W, Ross A R, Lograsso T A and Thiel P A 2002 *J. Phys.: Condens. Matter* **14** 2691
[16] Barman S R, Haberle P, Horn K, Maytorena J A and Liebsch A 2001 *Phys. Rev. Lett.* **86** 5108
[17] Shukla A K, Krüger P, Dhaka R S, Sayago D I, Horn K and Barman S R 2007 *Phys. Rev.* B **75** 235419
[18] Shukla A K, Biswas C, Dhaka R S, Das S C, Krüger P and Barman S R 2008 *Phys. Rev.* B **77** 195103
[19] McFeely F R, Kowalczyk S P, Ley L and Shirley D 1974 *Solid State Commun.* **15** 1051
[20] O'Brien W L and Toner B P 1995 *J. Vac. Sci. Technol.* A **13** 1544
[21] Tian D, Li H, Wu S C and Jona F 1992 *Phys. Rev.* B **45** 3749
[22] Zeng C, Zhu W, Erwin S C, Zhang Z and Weitering H H 2004 *Phys. Rev.* B **70** 205340
[23] Delaney D W, Bloomer T E and Lograsso T A 1997 *New Horizons in Quasicrystals* ed A Goldmann, D Sordelet, P A Thiel and J M Dubois (Singapore: World Scientific) pp 45–52
[24] Single crystals synthesized at the Materials Preparation Center. See www.mpc.ameslab.gov
[25] Shukla A K, Banik S, Dhaka R S, Biswas C, Barman S R and Haak H 2004 *Rev. Sci. Instrum.* **75** 4467
[26] Biswas C, Dhaka R S, Shukla A K and Barman S R 2007 *Surf. Sci.* **601** 609
[27] Buchanan J D R, Hase T P A, Tanner B K, Chen P J, Gan L, Powell C J and Egelhoff W F Jr 2002 *Phys. Rev.* B **66** 104427
[28] Seah M P and Dench W A 1979 *Surf. Interface Anal.* **1** 2
Briggs D and Seah M P 1990 *Practical Surface Analysis by Auger and X-Ray Photoelectron Spectroscopy* (New York: Wiley)
[29] Doniach S and Šunjić M 1970 *J. Phys. C: Solid State Phys.* **3** 287
[30] Yeh J J and Lindau I 1985 *At. Data Nucl. Data Tables* **32** 1
[31] Pan J S, Liu R S, Zhang Z, Poon S W, Ong W J and Tok E S 2006 *Surf. Sci.* **600** 1308
[32] Ley L, Dabbousi O B, Kowalczyk S P, McFeely F R and Shirley D A 1977 *Phys. Rev.* B **16** 5372
[33] Stadnik Z M 1999 *Physical Properties of Quasicrystals* (*Springer Series Solid State Science*) (Berlin: Springer)
[34] Shivaparan N R, Teter M A and Smith R J 2001 *Surf. Sci.* **476** 152
[35] Wuttig M, Gauthier Y and Blügel S 1993 *Phys. Rev. Lett.* **70** 3619
[36] Schieffer P, Krembel C, Hanf M C and Gewinner G J 1999 *J. Electron. Spectrosc. Relat. Phenom.* **104** 127
Schieffer P, Krembel C, Hanf M C and Gewinner G J 1998 *Phys. Rev.* B **57** 1141
[37] Rader O, Gudat W, Carbone C, Vescovo E, Blügel S, Klägases R, Eberhardt W, Wuttig M, Redinger J and Himpsel F J 1997 *Phys. Rev.* B **55** 5404
[38] Gierer M, Van Hove M A, Goldman A I, Shen Z, Chang S L, Jenks C J, Zhang C M and Thiel P A 1997 *Phys. Rev. Lett.* **78** 467
[39] Zheng J, Huan C H A, Wee A T S, Van Hove M A, Fadley C S, Shi F J, Rotenberg E, Barman S R, Paggel J J, Horn K, Ebert Ph and Urban K 2004 *Phys. Rev.* B **69** 134107
[40] Biswas C, Shukla A K, Banik S, Ahire V K and Barman S R 2003 *Phys. Rev.* B **67** 165416
[41] Fadley C S, Shirley D A, Freeman A J, Bagus P S and Mallow J V 1969 *Phys. Rev. Lett.* **23** 1397
Fadley C S and Shirley D A 1970 *Phys. Rev.* A **2** 1109
[42] Hillebrecht F, Jungblut R and Kiske E 1990 *Phys. Rev. Lett.* **65** 2450
[43] Veal B W and Paulikis A P 1983 *Phys. Rev. Lett.* **51** 1995